

Author Queries

Journal: Journal of the Royal Society Interface

Manuscript: rsif20100681

- Q1** The sentence 'Studies ...contribute' seems to be incomplete. Please check.
- Q2** Please check if the edit made to the sentence 'Photographs ... more than 5 s' is correct.
- Q3** Please check if the edit made to the sentence 'This factor ... same size' is correct.
- Q4** Please provide author and year details for the personal observation.

Capillary-based static self-assembly in higher organisms

Jonathan Voise^{1,*}, Michael Schindler^{2,†}, Jérôme Casas¹
and Elie Raphaël²

¹Université de Tours, IRBI UMR CNRS 6035, Parc Grandmont, 37200 Tours, France

²Laboratoire PCT, UMR Gulliver CNRS-ESPCI 7083, 10 Rue Vauquelin, 75231 Paris
Cedex 05, France

Organized structures produced by dynamic self-assembly are often observed in animal groups. Static self-assembly, however, has to date only been observed at the cellular and sub-cellular levels. The aim of this study was to analyse organized structures in immobile whirligig beetle groups on the water surface. We used theoretical and computational approaches to model the meniscus around whirligig beetles and to calculate the surface energy for configurations involving two beetles. Theoretical predictions were then tested using live insects and resin casts. Observations were also made for three and more casts. The meniscus of whirligig beetles had a bipolar shape with two concave parts. For two beetles, predicted configurations based on energy minima corresponded to beetles in contact by their extremities, forming lines and arrows, and agreed well with observations. Experimental results for three and more beetle casts revealed new geometrical arrangements similar to those obtained with colloids at interfaces. This study provides the first example of static self-assembly at the inter-organism level and shows importance of capillary interactions in such formations. We identify the ecological context in which our findings are of importance.

Keywords: air–water interface; capillary interactions; collective phenomena; colloids; whirligig beetles

1. INTRODUCTION

Living in groups is a common feature in organisms. Organized structures are often observed in such groups and they have been classified as self-assembly and self-organization [1–3]. *Self-assembly* is defined as a spontaneous formation of organized structures through a stochastic process that involves pre-existing components, which is reversible and may be controlled by proper design of the components, the environment and the driving force [4]. Two kinds of self-assembly can be distinguished—static and dynamic [3,4]. *Static* self-assembly leads to structures with local or global equilibrium, whereas *dynamic* self-assembly leads to stable structures that are not in equilibrium [4]. Using these definitions, *self-organization* in animal groups can be considered as a dynamic self-assembly phenomenon. Numerous examples of dynamic self-assembly of groups of organisms have been studied, such as fish schools and ant trails [1]. These phenomena can be produced by physical interactions [5], behavioural interactions [6] or both [7]. In contrast, static self-assembly has not been reported to occur between organisms. However, several examples have been found at lower organizational levels. The tobacco mosaic virus is a well-known example of static self-assembly in biological systems [8]. Other examples at the cellular or intracellular

level have been described, including the formation of filopodia and protein folding [9,10]. Static self-assembly also occurs in inorganic systems, and has been extensively studied for colloids (i.e. micro- or nano-particles) at interfaces [11].

Adult whirligig beetles (Coleoptera, Gyridae) exhibit several collective behaviours on the water surface that can be considered as dynamic self-assembly [12,13]. Whirligig beetles are semi-aquatic insects that have their body partially immersed in water; they have specific adaptations to this lifestyle, including divided composite eyes to see above and below the water surface [14], and floating antennae able to detect surface waves [15–17]. They are usually found in groups of 10 to several thousands of individuals [12]. The major advantage of swarming in these insects seems to be protection against predators [18,19]. Studies of the dynamics of the positions of individual within-whirligig beetle groups have shown that sex, satiation and predator attack each contribute [13,20]. Whirligig beetle swarms can contain only one single species or several species or, often, several genera [12,21]. The activity of individuals within groups is strongly affected by temperature, and warm beetles are more active [22]. Swarms of whirligig beetles, even species living on running water, stay in particular locations [12], and beetles forage on water by tracing circling trajectories. Whirligig beetles show periods of reduced activity, for example when basking [22], but

*Author for correspondence (jonathan.voise@etu.univ-tours.fr).

†These authors have contributed equally to the study.



Figure 1. A group of whirligig beetles (*Macrogyrus* spp.) resting on the water surface. Particular configurations can be observed, for example, the flower-like configuration on the top right corner (© Copyright Chris Shafer).

little is known about collective phenomena during these resting periods. Observations indicate however that immobile whirligig beetles aggregate in particular configurations, as shown in figure 1. This strongly suggests a static self-assembly phenomenon [23]. This view is supported by analogies with studies on colloids where self-assembled particles in equilibrium show similar patterns [24]. Several forces can drive static self-assembly between colloids, such as van der Waals interactions, electrostatic interactions and capillarity [25]. Given the size of whirligig beetles (larger than 3 mm) and the non-charged nature of these insects, it seems likely that their presumed self-assembly is capillary induced.

We investigated whether surface tension effects, capillarity in particular, can account for the observed patterns formed by resting whirligig beetles. We used theoretical and computational approaches to model the meniscus around a single beetle, and to estimate the surface energy associated with configurations between pairs of beetles. Resin casts of whirligig beetles were used to test the predictions obtained on the basis of surface energy minima, and to explore the range of configurations involving several beetles. The spatial arrangements can be adequately explained by the capillary interactions induced by the surface tension and our analysis supports the hypothesis of static self-assembly in whirligig beetles.

2. METHODS

2.1. Meniscus around whirligig beetles

The meniscus is a static deformation of an interface between two fluids and corresponds to equilibrium between capillary forces and gravity, minimizing the surface energy [26]. The shape of the meniscus around floating objects is strongly affected by their shape, weight and chemical properties [27,28]. The shape of the contact line is important for determining the meniscus around whirligig beetles, as will be shown below. The contact line (i.e. air–water–beetle interface) is defined by the margins of the elytra and the thorax,

and the hairs around the head (on the antennae and the labium, i.e. the extremity of the head) and around the pygidium (i.e. the extremity of the abdomen). The hairs of the pedicel, the floating part of the whirligig beetle antenna, are important for the buoyancy of the head [29]. The only information reported to date about the meniscus around whirligig beetles was provided by Larsen [23] who described its bipolar shape. The shape of the meniscus is responsible for capillary interactions between individuals.

2.2. Whirligig beetles

Whirligig beetles of the species *Gyrinus substriatus* Steph. were collected from a temporary pond in *Indre et Loire*, France. They were kept in 10 l aquariums, in groups of 8–10, and were fed daily with *Drosophila* fruitflies. Aquariums were filled with tap water, which was changed weekly. Beetles were placed on water in a $17 \times 15 \times 9$ cm aquarium with black walls facilitating the visualization of menisci, and photographed to analyse the shape of the meniscus that the beetles produced. Photographs were also taken through a stereomicroscope using dead beetles to measure the shape of the contact line. Beetles were photographed from the front, top and sides.

To study capillary interactions between whirligig beetles, several individuals were put together on water in a small aquarium ($15 \times 10 \times 5$ cm). The walls of the aquarium were plastic with a contact angle of approximately 90° (i.e. producing very little deformation of the surface) to avoid capillary interactions between walls and beetles. In normal laboratory conditions, it was difficult to observe immobile groups of beetles. To reduce their activity and thereby facilitate photography, the aquarium was placed in a cold chamber (6°C) for several hours. Photographs were taken once configurations involving two or more individuals were stable, lasting for more than 5 s.

2.3. Governing equations

When a whirligig beetle is immobile on the water surface, a meniscus corresponding to an equilibrium of the air–water interface is formed around the insect. This equilibrium configuration is governed by the balance of the free energy of surface tension and gravitational forces; each beetle deforms the surface around it owing to its weight and also to the form of its body. This equilibrium configuration can be determined by standard techniques of variational calculus, subject to boundary conditions. For each beetle, considered as a rigid floating object, six degrees of freedom are to be determined, namely the coordinates (C_x, C_y, C_z) of a reference point, which is fixed with respect to the floater and three rotation angles around it (φ, ψ, η ; figure 2). The surrounding air–water interface carries an infinite number of degrees of freedom, namely the full height profile of the free surface at all points. Upon variation, these degrees of freedom lead to the well-known Laplace law of curvature (equation (2.2) below). The rigid floaters and the free surface are coupled by the boundary condition (see below) at

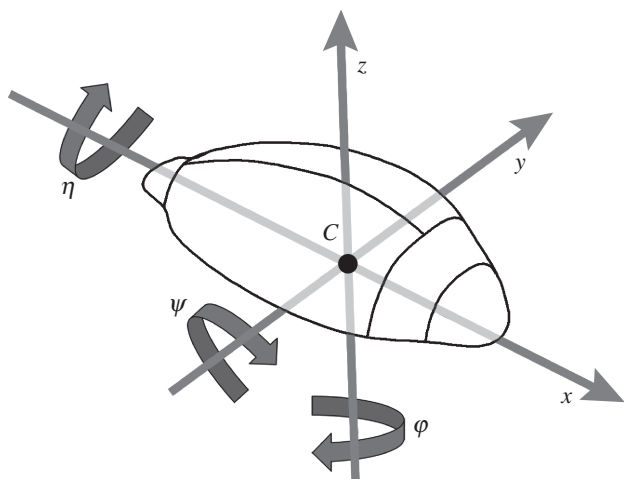


Figure 2. The six free degrees of freedom used in numerical analysis, position of the centre of the body (C) (x, y, z) and three angles (φ, ψ, η) that correspond to yaw, pitch and roll, respectively.

the contact curve where water, air and insect meet. We present here the equations which we subsequently solved numerically with the aid of *Surface Evolver* as described in §2.4.

The free-energy expression E , which is to be varied with respect to these degrees of freedom, is the sum of the free energy of the air–water interface, S_{AW} with surface tension γ , and of two terms accounting for gravity:

$$E = \gamma S_{AW} + g \int_{V_B} d\mathbf{r} r_z \rho_B(\mathbf{r}) + g \int_{V_W} d\mathbf{r} r_z \rho_W(\mathbf{r}). \quad (2.1)$$

The geometry of the model system is depicted in figure 3, where the volumes, interfaces and the normal vectors \mathbf{N} and \mathbf{n} are defined. The index B denotes the beetle, W stands for water and A for air; r_z is the vertical component of the vector \mathbf{r} , g the gravitational acceleration, and ρ_B and ρ_W denote the mass densities of the insect and of water, respectively. The density of air and the surface tensions of the other two interfaces (S_{AB} and S_{BW}) are not considered in equation (2.1). Usually, the meniscus is influenced by the angle of contact, but here there is no prescription for the contact angle because of the sharp edge of the contact line and of the probable chemical discontinuity between the wetted and un-wetted parts of the body [30–32]. We assume the contact line to be pinned at the margin of the elytra, which is, geometrically, sufficiently sharp to allow a wide range of contact angles Q4 (personal observation).

The variation is initially done with respect to all positions of all interfaces between the three volumes. On the interface S_{AW} , this variation leads to the Laplace equilibrium condition for height profile, surface tension and curvature κ at any point of the interface S_{AW}

$$[-\gamma\kappa + (r_z - z_0)g\rho_W] \mathbf{N} = 0. \quad (2.2)$$

The height offset z_0 is defined as the height of the surface far from all floaters, where the curvature vanishes. Then, in a subsequent step, the rigid-body constraints for the floater B are used. The resulting

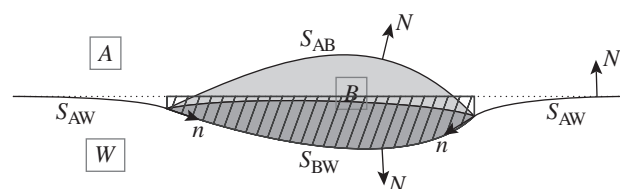


Figure 3. The geometrical annotations for volumes, surfaces and normal vectors, used in the equations. The volume B includes both parts of the floater, above and below the contact curve, which are shaded in different grey tones. The hatched area indicates the volume V^* , which enters the buoyancy force.

equilibrium conditions are implicit equations for the degrees of freedom, the position coordinates (C_x, C_y, C_z) and the angles (φ, ψ, η). The first set of equations, which can be used to determine \mathbf{C} , reads:

$$\begin{aligned} & -\gamma \oint_{C_{ABW}} \mathbf{n} - g \int_{V_B} [\rho_B \mathbf{e}_z + (r_z - z_0) \nabla \rho_B] \\ & + g \int_{S_{BW}} (r_z - z_0) \rho_W \mathbf{N} = 0. \end{aligned} \quad (2.3)$$

Here, \mathbf{n} is the vector normal to the contact curve but tangential to the air–water interface, S_{AW} . A similar set of equations, not given here, determines the angles.

Equation (2.3) comprises several integrals over geometrical entities; each depends on all six degrees of freedom of the floater. The first integral states that the surface tension pulls at the contact curve in the direction tangential to the water–air interface, and the second integral says that gravity pulls the floater in the z -direction with some modifications owing to mass distribution, which is not necessarily homogeneous. The third integral is the buoyancy force, which is not simply volume multiplied by density difference known from Archimedes’ principle for entirely submerged bodies, because the floater in this model system is only partially immersed, and the air–water interface is not flat. Further analysis of equation (2.3) allows a geometrical interpretation of Archimedes’ principle in the case of uniform density, ρ_B : by extending the contact line vertically up to the water level z_0 a volume V^* (the shaded volume in figure 3) can be defined. Only this part of the displaced fluid contributes to the buoyancy force, the remaining part above the free surface does not. The calculation and physical arguments for this shape are given by, for example, Keller [33] and Vella & Mahadevan [34].

The contact line, which is fixed by the morphology of whirligig beetles, constitutes a boundary condition to the surrounding free surface profile. Both curvature of the contact line and the insect weight contribute to determining the observed meniscus. The exact shape of the meniscus, the immersion depth of the reference point and the orientation angles all influence each other, as they are all implicitly present in equation (2.3). The asymmetric shape of the contact line also contributes. For the given shape of a whirligig beetle, for example, the equilibrium orientation is such that the head lies deeper than the extremity of the

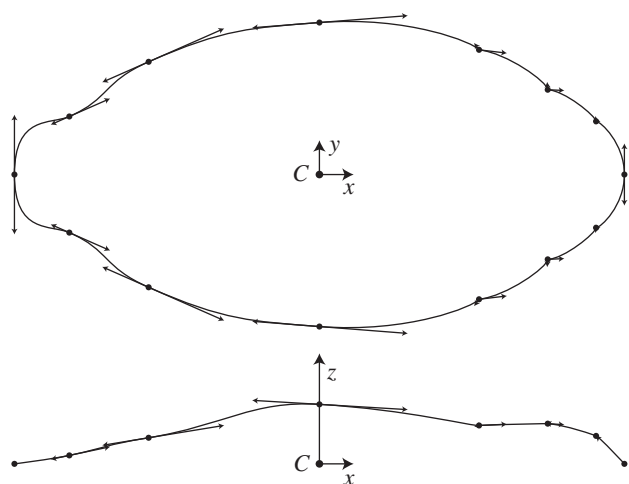


Figure 4. Top and side views of the contact line represented by cubic Bezier curves. The control points are indicated by black dots and arrows. Deformation along the z axis is amplified by a factor 3 to facilitate the visualization of the contact line.

abdomen—even if the mass density is assumed to be homogeneous. This orientation is thus solely a result of the shape of the contact curve.

The interaction between two or more whirligig beetles follows the same rules. The common meniscus of two floaters depends on both positions and rotations.

2.4. Solving equations with Surface Evolver

To investigate the shape of the meniscus for a single whirligig beetle and the interaction between two of them, we solved the above equations numerically. This was done using the program Surface Evolver [35], which discretizes the surface into triangles and searches to minimize the energy expression (2.1) by displacing the vertices of these triangles. Incorporating the experimentally observed geometry of the beetle (*G. substriatus*) into this framework was one of the major technical difficulties of the present work. It was done in three steps. First, the contact line was retraced on two-dimensional curves using top-view and side-view photos of a dead beetle. For simplification, details such as the hairs around the head and the abdomen, as well as the complex shape around the antennae were not taken into account. These two projected contact lines were then in turn used as input data for an optimization algorithm to find a three-dimensional representation in the form of Bezier curves. The optimization minimizes the overall mean-square distance between the projected inputs and the fitted curve. It strictly respects tangential constraints, which renders the representation sufficiently smooth. The parameters for the resulting 14 Bezier curves were then used as boundaries and constraints in the input file for Surface Evolver (figure 4). These boundaries and constraints were formulated in terms of the six free degrees of freedom described above, namely the coordinates of the reference point C and three angles (φ , ψ , η ; figure 2).

The calculation of the equilibrium conditions given in the previous section showed that each aspect of the

immersed insect morphology, and not only the contact line, affects the meniscus. In principle, a numerical simulation should therefore model the whole geometrical form of the beetle's body. This, however, is a tedious task, and is not likely to be fruitful without access to the mass distribution inside the whirligig beetles. Therefore, we considered that it would be sufficient for our aims to model only the contact line and to minimize the free energy for a fixed immersion depth, which was obtained from observations. The value of this fixed depth, 0.2 mm, was determined using side-view photos of living individuals on a water surface.

To investigate the static configurations between two whirligig beetles, Surface Evolver was used with two beetles (i.e. two contact lines) on the surface. The free energy as a function of their relative orientation was investigated by minimizing this energy with respect to the parameters C_x , C_y , ψ , η of both beetles, while the angle φ was held fixed during one minimization. A sweep over all φ values therefore yields information about the static equilibrium angles and about their respective free energies.

We considered three main configurations for two beetles: side, line and arrow. The *line* configuration corresponds to beetles with their bodies aligned in the same axis, and the *arrow* configuration corresponds to beetles in contact at their extremities with an angle between -90° and 90° between the two body axes. These contacts can be at the heads (*head/head*), abdomens (*back/back*) or both (*head/back*). The *side* configuration describes beetles with their body axes in parallel and in contact at their sides, oriented in the same direction (*head/head*) or in opposite directions (*head/back*). Several initial configurations, differing in their absolute position on the coordinate axes, give the same value of $\Delta\varphi$ which is a relative measure. Here, we used $\varphi_2 = -\varphi_1 + 180^\circ$ and $\varphi_2 = -\varphi_1 + 360^\circ$ for the two initial configurations that are head/head side and head/back side, respectively. This choice was made to limit the mesh deformation in numerical analysis.

2.5. Experiments using a physical model

To facilitate the comparison of the interactions between living beetles with the numerical analysis, we introduced an intermediate physical model reducing whirligig beetles to the morphological elements which govern the capillary attraction. Casts of *G. substriatus* were used as a physical model to avoid problems with the activity of lively swimming beetles. Moulds in silicon were made using dead dried beetles. Only the upper part of the elytra was outside the mould. Legs were removed because they could modify the contact line if too close to the margin of the elytra. Once moulds were dried, dead beetles were removed and coloured resin (Cristal resin, Gedeo; Vitrail paint, Pébéo) was injected with a syringe into the moulds, taking care to eliminate any air bubbles from the resin. Then, dried resin casts were extracted from the mould and surplus of resin was removed with a razor blade. Utilization of silicon and resin gave very accurate casts in terms of morphology. The upper part of the

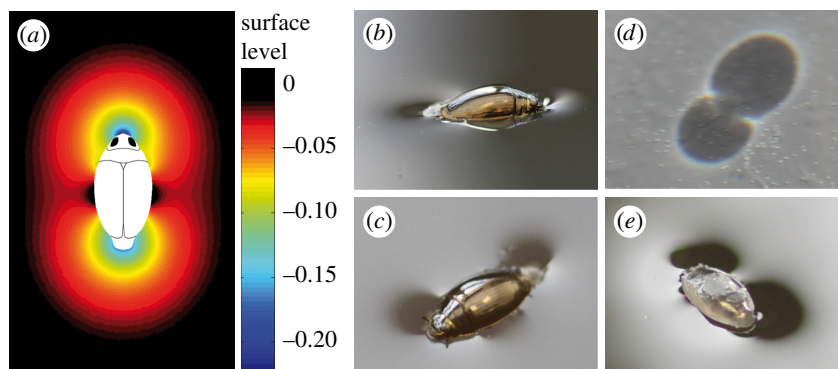


Figure 5. Static deformation of the water surface around whirligig beetles. (a) The bipolar meniscus around *Gyrimus substriatus* was calculated numerically. (b–e) Photos of the meniscus obtained experimentally with (b–d) living beetles and (e) resin casts. (c) Shadow of the meniscus at the bottom of the aquarium. The scale bar in (a) represents 5 mm.

elytra was not moulded, but it has no importance for this study because this part was always out of water and sufficiently far from the contact line to have no influence on the meniscus shape or on capillary interactions. Casts were then soaked in hot wax to compensate for their hydrophilic property and the absence of hairs at the front and back. This process rendered the cast hydrophobic and conferred the appropriate buoyancy. The buoyancy was verified using side view photos of a floating cast: the shape and the depth of the contact line were similar to that observed for living beetles. To maintain this buoyancy, casts were re-soaked in wax after each experiment. Moulds were made with 10 beetles and each was used to make one or two casts. The mean weight of the casts (201 mg, 10 individuals) was higher than that of living beetles (150 mg, 10 individuals), but, as mentioned previously, the buoyancy was not affected. We verified that the shape of the meniscus formed by the casts was appropriate by studying photos of casts on the water surface under the same conditions as for living beetles. Profile photos on water surface were also taken to make sure that the contact line was consistent with that observed for living beetles.

To study configurations owing to capillary interactions, casts were placed on the water surface, in a Petri dish whose walls made a contact angle of approximately 90° with water. Configurations were photographed for two, three and more than 10 casts. Two hundred configurations with two casts and 30 with three casts were photographed. As for living beetles, photos were taken when configurations were static for more than 5 s.

3. RESULTS AND DISCUSSION

3.1. Meniscus shape

The meniscus around a single beetle, calculated numerically, is shown in figure 5a. The meniscus had a bipolar shape with two concave parts, one at the front and one at the back of the insect. The menisci at the front and back of the body were of similar sizes (approx. 5 mm). However, the concave part around the head (minimum = -0.22 mm) was deeper than that around the pygidium (minimum = -0.16 mm).

The shape of the meniscus around live whirligig beetles observed experimentally is shown in figure 5b,c. The two concave parts, at the front and back, were clearly visible. The shadow of the meniscus at the bottom of the aquarium (figure 5d) confirmed its bipolar shape. The meniscus produced by our physical model (resin casts of whirligig beetles; figure 5e) had the same bipolar shape as that produced by living beetles.

These experimental results validated the theoretical modelling of the meniscus around whirligig beetles and are in agreement with the early observation of Larsen [23] who noticed a bipolar shape. Only the shape of the contact line, defined by the insect's morphology, and the sinking of the top of the contact line into water were used for modelling the meniscus. Thus, we can conclude that the shape of the meniscus is mainly owing to the weight and morphology of whirligig beetles. Although the chemical properties of the cuticle might have an influence on the meniscus [36], the meniscus could be modeled without this effect. The importance of the insect morphology is owing to the sharp edge around the body delimiting the contact line: a sharp edge of this type allows variations in the contact angle which changes to minimize the surface energy [31]. The overall shape of the contact line along the body axis is a convex curve with its maximum at the middle of the body (figure 4). The amplitude of this curve is relatively small (0.2 mm) but sufficient for determining the shape of the meniscus.

3.2. Capillary interactions

The free energy E as a function of the angle $\Delta\varphi = \varphi_2 - \varphi_1$ between two beetles (figure 6a) is shown in figure 6b,c. The head/head side starting configuration (figure 6b) exhibits three energy minima upon varying $\Delta\varphi$. The global minimum ($\Delta\varphi = -180^\circ$) was the head/head line configuration. Another line configuration, the back/back line ($\Delta\varphi = 180^\circ$), corresponded to a shallow local minimum. Another local minimum was found for $\Delta\varphi = 58^\circ$, corresponding to the back/back arrow configuration. Other configurations are unstable and lead to one of these three minima. For the second starting configuration (figure 6c), the energy curve was symmetric. Again, three minima were obtained, a wide one for the head/back

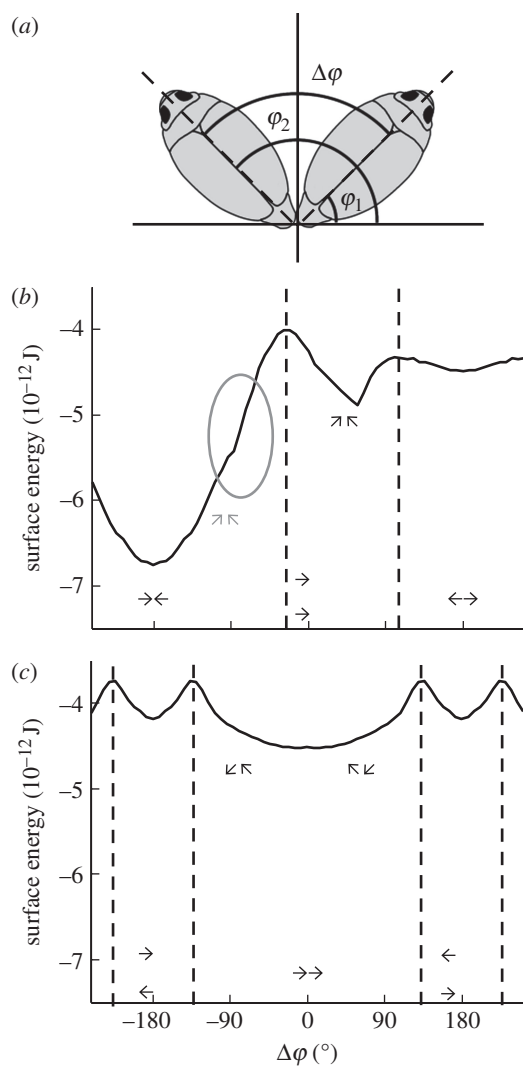


Figure 6. Numerically calculated surface energy as a function of the configuration of two beetles. (a) Configurations are characterized by the relative angle $\Delta\varphi = \varphi_2 - \varphi_1$ (in this example $\varphi_2 = 135^\circ$; $\varphi_1 = 45^\circ$; $\Delta\varphi = 90^\circ$). (b,c) Surface energy as a function of $\Delta\varphi$ for initial configurations corresponding to head/head side ($\Delta\varphi = 0^\circ$) and head/back side ($\Delta\varphi = -180^\circ$; $\Delta\varphi = 180^\circ$), respectively. Surface energy is represented as the value for a given $\Delta\varphi$ minus the surface energy for two beetles separated by a substantial distance (i.e. the same surface without interaction between the two menisci). Dashed lines delimitate the basins of attraction (i.e. the ranges of $\Delta\varphi$ leading to one energy minimum). Arrows show the configurations of the two beetles, each arrow representing one beetle, with the point corresponding to the head. The grey ellipse in (b) shows an expected basin of attraction corresponding to a head/head arrow configuration, which is not predicted by our computations.

line configuration ($\Delta\varphi = 0^\circ$), and two other minima at $\Delta\varphi = -180^\circ$ and $\Delta\varphi = 180^\circ$ corresponding to the starting configuration, i.e. head/back side configuration.

Static configurations involving two living beetles obtained experimentally are represented in figure 7a–c. We observed both line configurations (figure 7a) and arrow configurations (figure 7b). Side configurations were never observed. However, another configuration was observed, corresponding to a combination of the line and the side configuration, called hereafter the *line-side*

configuration (figure 7c). The number of observations was however too small for quantitative analysis.

The configurations adopted by pairs of resin casts were evaluated and compared with predictions (table 1). Line (67.5%) and arrow (27.5%) configurations were the most frequently observed (figure 7d,e). Line-side configurations (figure 7f) were rare (5%) and side configurations did not occur.

3.3. Predicted and observed frequencies for pair configurations

The free energy profile $E(\Delta\varphi)$ can be used to assess the probability of finding a pair of beetles in any given angular configuration, provided that they are subject to random perturbations. Under these conditions, the probabilities are proportional to $\exp(-E/k_B T)$, where T is an effective temperature and k_B is the Boltzmann constant. This can be used to predict how frequently the indicated line or arrow orientations should be observed. There is one important caveat, however, as the random perturbations must be sufficiently large for the system to pass from one local minimum to another. Simple thermal noise is not sufficient, as the energy barriers between the minima are of the order of $10^6 k_B T$ with the ambient temperature T at 20°C (figure 6). However, in field conditions, capillary waves produced by wind and other animals may provide sufficient perturbations and allow changes in configuration from one minimum to another.

Qualitative interpretation of the values of table 1 is nevertheless possible. They do not result from randomly driven passage from one minimum to another on the energy landscape of figure 6, which is the minimal energy of a final equilibrium state. The statistics were obtained by randomly putting two casts on the water surface and noting the final configuration. In the space spanned by all possible initial configurations (distances and angles), there are thus *basins of attraction* of the observed final configurations. The size of these basins in the high-dimensional initial space gives us the probabilities in table 1, because the pathway from any initial configuration to the corresponding final one can be assumed to be deterministic (see above the smallness of $k_B T$ compared with E). Indeed, the two casts approach each other, turning if necessary, and then come into contact. Only this final contact state is described by the free energy curve in figure 6. Once in contact, further minimization of the free energy is readily trapped even by tiny local minima not visible on the plot, as long as they are much larger than $k_B T$. This is the case for the head/head arrow configuration at about $\Delta\varphi = -90^\circ$, which was observed but not predicted as a minimum of energy (table 1). A local minimum is likely to exist there (figure 6b, grey ellipse) owing to small shape variations which are not resolved by our numerical model.

A conceptual view of the basins of attraction is shown schematically in figure 8. The drawing was compiled from general symmetry considerations, including the invariance under exchange of the two beetles and the periodicity of the angles. We simplified the high-dimensional space of initial states to the two initial φ

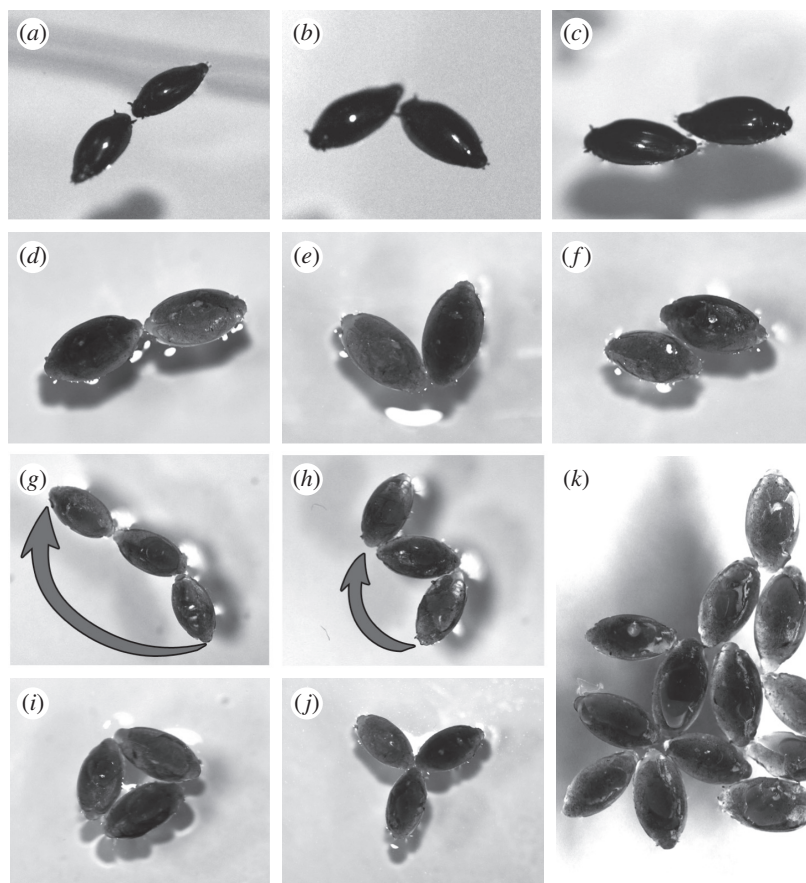


Figure 7. Static configurations obtained experimentally with (a–c) living whirligig beetles and (d–k) resin casts. With two individuals, (a,d) lines, (b,e) arrows and (c,f) line/side configurations were observed. With three individuals, lines and arrows were observed, as well as two new configurations—(i) flower and (j) triangle. Arrows indicate how the configurations change if the water is slightly agitated: (g) lines give (i) triangles, whereas (h) double arrows (j) give flowers.

Table 1. Static configurations between two whirligig beetles, with theoretical predictions regarding the surface energy (min, minima; unst, unstable) and recording of observations made with resin casts (obs, observed; Ø, not observed; 200 observations). Each arrow represents a beetle, the tip corresponding to the head. Data from line–side configurations are grouped together.

	line			arrow			side			line–side		
	←→	→←	→→	↖↗	↓↓	↓↗	→→	→←	←→	→←	→→	
prediction	min	min	min	min	unst	min	unst	min	—	—	—	
observation	obs	obs	obs	obs	obs	obs	Ø	Ø	obs	obs	obs	
%	17.5	18.5	31.5	4.5	14.0	9.0	0	0	5.0	5.0	5.0	

angles, such that the initial distance is the same for all trajectories, and assuming that the other orientation angles (ψ and η ; figure 2) do not have a substantially different effect. The starting element of the drawing was the centres of the basins corresponding to line configurations (i.e. each multiple of 180° for φ_1 and φ_2 ; e.g. see the white cross on figure 8), and then considerations from numerical and experimental results. To relate calculated numerical results (figure 6) to this drawing, dashed lines represent the $\Delta\varphi$ axes $[-180, 180]$ of figure 6b,c, where the sum $\varphi_1 + \varphi_2$ is a constant: short-dashed lines represent the $\Delta\varphi$ axes of figure 6b ($\varphi_1 + \varphi_2 = 180^\circ$) and the long-dashed line represents the $\Delta\varphi$ axes of figure 6c ($\varphi_1 + \varphi_2 = 360^\circ$). The basins of attraction are represented as a function of φ_1

and φ_2 . Figure 8 allows us to explore a larger number of initial conditions (including similar values of $\Delta\varphi$), for which numerical computation would be too time consuming. The important feature of this drawing is that the head/back line basin occurs twice (one full basin plus four quarters) and other line states occur once (two half basins). This factor of two is clearly seen in the observed frequencies (table 1), which indicate that all basins of attraction to the line states are of approximately the same size. The same argument applies to the arrow states that surround the line states. Again, we observe two occurrences of the head/back arrow, but only one of the back/back arrow, similarly reflected in table 1. Thus, the basins of attraction of these two configurations have the

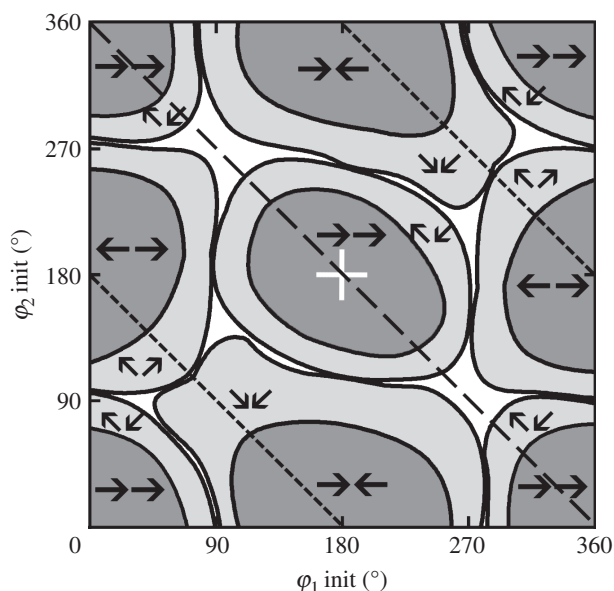


Figure 8. Conceptual representation of the basins of attraction of the surface energy as a function of the initial angles φ_1 and φ_2 of two beetles. Each arrow represents one beetle, the tip corresponding to the head. Dashed lines correspond to the $\Delta\varphi$ axes in figure 6: short-dashed lines represent $\varphi_1 + \varphi_2 = 180^\circ$ (figure 6*b*), and the long-dashed line represents $\varphi_1 + \varphi_2 = 360^\circ$ (figure 6*c*). Light and dark grey correspond to line and arrow configurations, respectively. White areas represent configurations for which we do not know the corresponding basin of attraction. The white cross gives an example of the centre of a basin of attraction corresponding to line configurations. The centres of other line basins are on the edges of the graph, and are not represented here.

same size. Only the head/head arrow state is different, as it was found much more often (table 1).

Differences between prediction and observation (i.e. for the head/head arrow and head/back side configurations) may also result from beetles in the numerical analysis all having exactly the same shape and the same length, whereas casts showed some variability in shape and size. For ellipsoidal colloids, Loudet & Poulin [37] showed that asymmetry of size between two colloids led to energy minima different from those for identical colloids. The same may apply to our whirligig beetle model.

3.4. Explorations with three and more beetles

With three casts, four configurations were observed. Line and arrow configurations appeared again (figure 7*g,h*). Arrows could be simple (two casts in line and two casts in arrow) or double (two arrows in opposite direction). Two new configurations were observed, a *triangle* and a *flower* (figure 7*i,j*). When more than 10 casts were placed on the water surface, static configurations included only flower and triangular configurations (figure 7*k*): lines and arrows were observed only as transitions. Slight agitation of water with a wire revealed that flower and triangular configurations were very stable (no change in configuration), whereas line and arrow configurations were unstable. Furthermore, following agitation, line configurations changed into triangles, and arrow configurations

became flowers (figure 7*g-j*). The analogy with capillary interactions described for colloids is very strong. Fournier & Galatola [38] investigated theoretical configurations induced by capillary interactions between spherical colloids having a quadrupolar meniscus. They found three configurations corresponding to minima of the surface energy: the line, the flower and the triangle configurations. They also found that triangles and flowers are more stable than lines, consistent with our experiments in whirligig beetles. Experimental studies with ellipsoidal colloids with a quadrupolar meniscus showed that shape-induced capillary interactions could produce dense networks of colloids with typical flowers and triangular configurations [24].

3.5. Ecological implications

As the shape of the meniscus is mainly determined by the insect's morphology, it is likely that the shape observed provides some advantages. First, capillary interactions between the head of whirligig beetles and potential prey may be advantageous because their menisci have the same shape and this will facilitate prey capture. Indeed, the majority of small arthropods falling on the water surface will form a concave meniscus because of their density and hydrophobic cuticle [30,39]. The shape of the meniscus could also facilitate mating. Whirligig beetles mate on the water surface [40], and the attractive capillary interaction between the head of the male and the abdomen of the female could facilitate mounting of the female by the male. In contrast, the concave parts of the meniscus could severely impede leaving the water. The meniscus on water banks is in general convex, leading to a repulsive interaction with the concave parts of the beetle meniscus. Other insects have developed morphological and behavioural adaptations to climb the meniscus at water edges [41], and it would be interesting to investigate how whirligig beetles do this. The bipolar meniscus of whirligig beetles could also be a problem if dust or pollen grains are present on the water surface: the concave parts attract such small particles which would then accumulate around the head and the pygidium. Dust around the antennae may disturb perception of surface waves. This could explain why whirligig beetles are often found on clean water and avoid dirty water surfaces.

We conclude that a capillary-based collective phenomenon occurs when resting whirligig beetles collect in swarms. Capillary interactions result in attractive forces and the assembling of individuals into a cohesive group. This group cohesion may enhance the reaction of an entire group of basking beetles faced with predators, and have only a low energetic cost. Indeed, field observations indicate that when a resting group of whirligig beetles is disturbed, the group reacts quickly with flight behaviour and returns to resting configurations after few seconds (personal observation). Results of the meniscus modelling indicate that resting whirligig beetles should interact up to 1 cm from each other. Experiments with resin casts showed that individuals could interact even up to 2 cm, which remains a short-range distance. Of course, theoretically the beetle menisci should interact across infinitely large distances

given an ideally flat water surface and an indefinite amount of time. However, in field and laboratory conditions, the range of attractive interactions should not be more than a few centimetres.

When there are only a few individuals active in a swarm, a combination of static (i.e. capillary-based) and dynamic self-assembly can occur. Active beetles often touch resting individuals and may break self-assembled structures. We could therefore observe a chain reaction in this situation, i.e. some individuals stay active for a few seconds, which is enough to excite some resting individuals, which will in turn excite other individuals. If the water surface is sufficiently calm locally, capillary-induced structures could then be re-formed. The proportion of static and dynamic self-assembly will depend on the proportion of active individuals in a given population.

4. CONCLUSION

As the same configurations were observed for living beetles and resin casts, we conclude that the formation of these structures is a passive and spontaneous phenomenon. Moreover, the configurations observed experimentally corresponded to those associated with global or local minima of the theoretical surface energy, indicating that whirligig beetles assembled according to predictable and physical constraints. Previous studies have shown that collective phenomena in lower organisms can be explained by physics alone. For example, non-equilibrium phenomena produced by bacteria in suspension can be adequately explained by hydrodynamic interactions alone [5]. Here, we found that organized structures in semi-aquatic insects can be predicted and reproduced with reference to surface tension phenomena.

Thus, the collective phenomenon of pattern forming by resting whirligig beetles corresponds to static self-assembly. As far as we are aware, this is the first described example of static self-assembly at the organism level, i.e. between individuals. This concept could be extended to individuals of different species; indeed, whirligig beetle aggregations often include several species and even several genera [12,21]. We believe that this phenomenon between organisms has not previously been described because the forces usually involved in static self-assembly are generally too weak to act significantly on higher organisms, for which gravity is the dominant force. Static self-assembly can occur for whirligig beetles because these insects live at the air–water interface, where capillary interactions both outweigh gravity effects and act at long range with respect to the size of the insects.

We would like to thank Sylvain Pincebourde for discussions. This work is part of the PhD thesis of J.V. financed by the Région Center under the supervision of J.C. This study was also financed by the RTP Bionique (CNRS).

REFERENCES

1 Camazine, S., Deneubourg, J.-L., Franks, N. R., Sneyd, J., Theraulaz, G. & Bonabeau, E. 2001 *Self-organization in*

- biological systems*. Oxfordshire, UK: Princeton University Press. 1072
- 2 Sendova-Franks, A. B. & Franks, N. R. 1999 Self-assembly, self-organization and division of labour. *Phil. Trans. R. Soc. Lond. B* **354**, 1395–1405. (doi:10.1098/rstb.1999.0487) 1073
- 3 Whitesides, G. M. & Grzybowski, B. 2002 Self-assembly at all scales. *Science* **295**, 2418–2421. (doi:10.1126/science.1070821) 1074
- 4 Pelesko, J. A. 2007 *Self assembly: the science of things that put themselves together*. New York, NY: Chapman & Hall/CRC. 1075
- 5 Baskaran, A. & Marchetti, M. C. 2009 Statistical mechanics and hydrodynamics of bacterial suspensions. *Proc. Natl Acad. Sci. USA* **106**, 15 567–15 572. (doi:10.1073/pnas.0906586106) 1076
- 6 Sumpter, D. J. T. 2006 The principles of collective animal behaviour. *Phil. Trans. R. Soc. B* **361**, 5–22. (doi:10.1098/rstb.2005.1733) 1077
- 7 Ishikawa, T. 2009 Suspension biomechanics of swimming microbes. *J. R. Soc. Interface* **6**, 815–834. (doi:10.1098/rsif.2009.0223) 1078
- 8 Fraenkel-Conrat, H. & Williams, R. C. 1955 Reconstitution of active tobacco mosaic virus from its inactive protein and nuclei acid components. *Proc. Natl Acad. Sci. USA* **41**, 690–698. (doi:10.1073/pnas.41.10.690) 1079
- 9 Lee, K., Gallop, J. L., Rambani, K. & Kirschner, M. W. 2010 Self-assembly of filopodia-like structures on supported lipid bilayers. *Science* **329**, 1341–1345. (doi:10.1126/science.1191710) 1080
- 10 Vendruscolo, M., Zurdo, J., MacPhee, C. E. & Dobson, C. M. 2003 Protein folding and misfolding: a paradigm of self-assembly and regulation in complex biological systems. *Phil. Trans. R. Soc. Lond. A* **361**, 1205–1222. (doi:10.1098/rsta.2003.1194) 1081
- 11 Bergström, L. 2006 Structures and formation of particle monolayers at liquid interfaces. In *Colloidal particles at liquid interfaces* (ed. B. P. Binks), pp. 77–107. New York, NY: Cambridge University Press. 1082
- 12 Heinrich, B. & Vogt, F. D. 1980 Aggregation and foraging behavior of whirligig beetles (Gyrinidae). *Behav. Ecol. Sociobiol.* **7**, 179–186. (doi:10.1007/BF00299362) 1083
- 13 Romey, W. L. & Galbraith, E. 2008 Optimal group positioning after a predator attack: the influence of speed, sex, and satiation within mobile whirligig swarms. *Behav. Ecol.* **19**, 338–343. (doi:10.1093/beheco/arm138) 1084
- 14 Hatch, M. H. 1927 The morphology of Gyrinidae. *Pap. Mich. Acad. Sci. Arts Lett.* **7**, 311–350. 1085
- 15 Eggers, F. 1926 The presumed function of Johnston's sensory organ in *Gyrinus*. *Zool. Anz.* **68**, 184–192. 1086
- 16 Eggers, F. 1927 Further information on the Johnston's sensory organ and avoidance ability of whirligig beetles. *Zool. Anz.* **71**, 136–156. 1087
- 17 Wilde, J. D. 1941 Contribution to the physiology of the Johnston organ and its part in the behavior of the *Gyrinus*. *Arch. Neer. de Physiol.* **25**, 381–400. 1088
- 18 Vulinec, K. & Miller, M. C. 1989 Aggregation and predator avoidance in whirligig beetles (Coleoptera, Gyrinidae). *J. N. Y. Entomol. Soc.* **97**, 438–447. 1089
- 19 Watt, P. J. & Chapman, R. 1998 Whirligig beetle aggregations: what are the costs and the benefits? *Behav. Ecol. Sociobiol.* **42**, 179–184. (doi:10.1007/s002650050429) 1090
- 20 Romey, W. L. & Wallace, A. C. 2007 Sex and the selfish herd: sexual segregation within non-mating whirligig groups. *Behav. Ecol.* **18**, 910–915. (doi:10.1093/beheco/arm057) 1091
- 21 Realzola, E., Cook, J. L., Cook, T. J. & Clopton, R. E. 2007 Composition of gyrinid aggregations in the east Texas primitive big thicket (Coleoptera: Gyrinidae). 1092

- 1135 *Coleopt. Bull.* **61**, 495–502. (doi:10.1649/0010-
1136 065X(2007)61[495:COGAI]2.0.CO;2)
- 1137 22 Fitzgerald, V. J. 1987 Social-behavior of adult whirligig
1138 beetles *Dineutus nigrior* and *D. discolor* (Coleoptera, Gyr-
1139 inidae). *Am. Midl. Nat.* **118**, 439–448. (doi:10.2307/
1140 2425801)
- 1141 23 Larsen, O. 1966 On the morphology and function of the
1142 locomotor organs of the Gyrinidae and other Coleoptera.
1143 *Opuscula Entomol. Suppl.* **30**, 1–241.
- 1144 24 Madivala, B., Fransaeer, J. & Vermant, J. 2009 Self-assem-
1145 bly and rheology of ellipsoidal particles at interfaces.
1146 *Langmuir* **25**, 2718–2728. (doi:10.1021/la803554u)
- 1147 25 Butt, H. J., Graf, K. & Kappl, M. 2006 *Physics and chem-
1148 istry of interfaces*. Weinheim: WILEY-VCH.
- 1149 26 de Gennes, P. G., Brochard-Wyart, F. & Quéré, D. 2003
1150 *Capillary and wetting phenomena: drops, bubbles, pearls
1151 and waves*. Berlin, Germany: Springer.
- 1152 27 Bowden, N., Arias, F., Deng, T. & Whitesides, G. M. 2001
1153 Self-assembly of microscale objects at a liquid/liquid inter-
1154 face through lateral capillary forces. *Langmuir* **17**, 1757–
1155 1765. (doi:10.1021/la001447o)
- 1156 28 Lewandowski, E. P., Bernate, J. A., Tseng, A., Searson,
1157 P. C. & Stebe, K. J. 2009 Oriented assembly of anisotropic
1158 particles by capillary interactions. *Soft Matter* **5**, 886–890.
1159 (doi:10.1039/b812257a)
- 1160 29 Kolmes, S. A. 1983 Ecological and sensory aspects of prey
1161 capture by the whirligig beetle *Dineutus discolor* (Coleop-
1162 tera, Gyrinidae). *J. N. Y. Entomol. Soc.* **91**, 405–412.
- 1163 30 Holdgate, M. W. 1955 The wetting of insect cuticles by
1164 water. *J. Exp. Biol.* **32**, 591–617.
- 1165 31 Oliver, J. F., Huh, C. & Mason, S. G. 1977 Resistance to
1166 spreading of liquids by sharp edges. *J. Colloid Interface
1167 Sci.* **59**, 568–581. (doi:10.1016/0021-9797(77)90052-2)
- 1168 32 Ondarcuhu, T., Fabre, P., Raphael, E. & Veyssie, M.
1169 1990 Specific properties of amphiphilic particles at fluid
1170 interfaces. *J. Phys. (Paris)* **51**, 1527–1536.
1171
- 1172 33 Keller, J. B. 1998 Surface tension force on a partly
1173 submerged body. *Phys. Fluids* **10**, 3009–3010. (doi:10.
1174 1063/1.869820)
- 1175 34 Vella, D. & Mahadevan, L. 2005 The ‘Cheerios effect’.
1176 *Am. J. Phys.* **73**, 817–825. (doi:10.1119/1.1898523)
- 1177 35 Brakke, K. 1992 The Surface Evolver. *Exp. Math.* **1**, 141–165.
1178
- 1179 36 Bush, J. W. M., Hu, D. L. & Prakash, M. 2007 The integu-
1180 ment of water-walking arthropods: form and function. In
1181 *Advances in insect physiology: insect mechanics and control*,
1182 vol. 34 (eds J. Casas & S. J. Simpson), pp. 117–192.
1183
- 1184 37 Loudet, J. C. & Pouligny, B. 2009 Self-assembled capillary
1185 arrows. *EPL* **85**, 28003. (doi:10.1209/0295-5075/85/28003)
- 1186 38 Fournier, J. B. & Galatola, P. 2002 Anisotropic capillary
1187 interactions and jamming of colloidal particles trapped
1188 at a liquid-fluid interface. *Phys. Rev. E* **65**, 031601.
1189 (doi:10.1103/PhysRevE.65.031601)
- 1190 39 Vincent, J. F. V. & Wegst, U. G. K. 2004 Design and
1191 mechanical properties of insect cuticle. *Arthropod Struct.
1192 Dev.* **33**, 187–199. (doi:10.1016/j.asd.2004.05.006)
- 1193 40 Kolmes, S. A. 1983 Precopulatory behavior of the whirligig
1194 beetle *Dineutus discolor* (Coleoptera: Gyrinidae). *J. N. Y.
1195 Entomol. Soc.* **91**, 273–279.
1196
- 1197 41 Hu, D. L. & Bush, J. W. M. 2005 Meniscus-climbing
1198 insects. *Nature* **437**, 733–736. (doi:10.1038/nature03995)
- 1199
- 1200
- 1201
- 1202
- 1203
- 1204
- 1205
- 1206
- 1207
- 1208
- 1209
- 1210
- 1211
- 1212
- 1213
- 1214
- 1215
- 1216
- 1217
- 1218
- 1219
- 1220
- 1221
- 1222
- 1223
- 1224
- 1225
- 1226
- 1227
- 1228
- 1229
- 1230
- 1231
- 1232
- 1233
- 1234
- 1235
- 1236
- 1237
- 1238
- 1239
- 1240
- 1241
- 1242
- 1243
- 1244
- 1245
- 1246
- 1247
- 1248
- 1249
- 1250
- 1251
- 1252
- 1253
- 1254
- 1255
- 1256
- 1257
- 1258
- 1259
- 1260